Dependence of Nonlinear Elastic Parameters of Consolidated Granular Media on Temperature in the Ambient Range

Ghorbani Ghezeljehmeidan, Amir; Kober, Jan ; Scalerandi, Marco; Zeman, Radovan

Important note
To cite this publication, please use the final published version (if applicable).
Please check the document version above.

Article

Dependence of Nonlinear Elastic Parameters of Consolidated Granular Media on Temperature in the Ambient Range

Amir Ghorbani Ghezeljehmeidan [1], Jan Kober [2], Marco Scalerandi [3,*] and Radovan Zeman [2,4]

1   Department of Microelectronics, Delft University of Technology, 2628 CD Delft, The Netherlands; amir.ghorbani@tudelft.nl
2   Institute of Thermomechanics of the Czech Academy of Sciences, 182 00 Prague, Czech Republic; kober@it.cas.cz (J.K.); rzeman@it.cas.cz (R.Z.)
3   Department of Applied Science and Technology, Condensed Matter Physics and Complex Systems Institute, Politecnico di Torino, 10129 Torino, Italy
4   Faculty of Nuclear Sciences and Physical Engineering, Czech Technical University in Prague, 115 19 Prague, Czech Republic
*   Correspondence: marco.scalerandi@polito.it

Abstract: Hysteretic nonlinear elasticity is often observed in consolidated granular media, including concrete, mortar, sandstones, or rocks. Nonlinearity is frequently quantified using Nonlinear Resonant Ultrasonic Spectroscopy (NRUS), which provides tools to define nonlinear parameters for both fast and slow dynamic effects, often observed when analyzing the propagation velocity dependence on strain in such materials. The dependence of these parameters on temperature was studied with the aim of using NRUS to quantify the induced thermal damage; thus, experiments were performed spanning a wide temperature range. However, since most of these materials are used in construction (concrete and sandstone, mostly), it is of interest to understand how sensitive the measured nonlinear parameters are to small environmental temperature fluctuations. In this paper, the dependence on temperature of elastic parameters is investigated, both linear (wave velocity and damping) and nonlinear (the slope and hysteresis of the curves describing the strain dependence of wave velocity and residual conditioning effect on wave velocity), separating the slow from the fast dynamic properties of nonlinearity. The observations reported here denote a different behavior for concrete and Berea sandstone.

Keywords: nonlinear resonant ultrasonic spectroscopy; sandstones; nonlinear wave velocity; temperature dependence

1. Introduction

Consolidated granular media, which are frequently utilized in construction and building technology (e.g., rocks and sandstones [1–4], concrete [5,6], mortar [7], etc.), exhibit a strong nonlinear elastic behavior, which is often significantly enhanced when damage is present. Such behavior is characterized by the presence of hysteresis in the dependence of the wave velocity and damping on strain, which might be seen as originated by slow dynamics [8–12]. The latter is indeed the main evidence of hysteresis and memory effects. This phenomenon is due to the existence of the equilibrium states of the material, characterized by given viscoelastic properties (modulus [13] and damping [14]), which are dependent on the strain applied (drive strain amplitude). The relaxation to such an equilibrium state is a long-term relaxation process, which could be described as a multirelaxation phenomenon [15–17].

Nonlinear elastic hysteresis is often evident even at low strain levels (of the order of 10^{-7}), with variations in the propagation velocity of the order of percent (and much higher damping variations). Several techniques have been developed to detect such a small nonlinearity, mostly applicable to small samples: Nonlinear Resonant Ultrasound Spectroscopy—NRUS [18–20]; the Scaling Subtraction Method—SSM [21,22], Nonlinear Elastic Wave Spectroscopy [23,24], etc. All these methods show that the nonlinear effects are significantly stronger when materials are damaged, thus providing an efficient tool for nondestructive testing.

Studies reported in the literature show the strong sensitivity of nonlinear parameters to damage evolution: quasi-static loading-induced damage [25,26], thermal damage [27–29], chemical damage [30–32], etc. However, to make nonlinear ultrasonic methods a tool to quantify damage, it is necessary to separate the nonlinearity increase due to microstructural changes from those due to environmental effects (in the environmental range). While some studies have been reported to study humidity's effects on the hysteretic elasticity [18,33–35], fewer studies are devoted to analyze temperature effects.

Most of them include thermal damage to the material [27–29] or aim to analyze how temperature changes might induce slow dynamic effects [36,37]. Some studies have reported the effects of temperature inducing low levels of damage [29] or have monitored the evolution of nonlinear rock parameters while the temperature varies, i.e., not at equilibrium [38]. On the contrary, results are available showing the dependence of linear elastic parameters on temperature [39,40].

Here, the work focuses on analyzing the dependence of linear and nonlinear elastic parameters in the environmental temperature range, avoiding transient regimes. Concrete and sandstone samples have been studied, with the aim of quantifying the influence of temperature on the measured nonlinearity and, in particular, its order of magnitude compared to the order of magnitude of damage-induced nonlinearity variations. In Section 2, details about the experiment and material tested are given, together with a recap on the NRUS method. The results are reported in Section 3. The temperature dependence of the linear and nonlinear elastic parameters is discussed in Section 4, while the discussion and conclusions are reported in Section 5.

2. Material and Methods

2.1. Materials and Set-Up

Berea sandstone sample and a concrete sample were tested. The former was in the shape of a thin cylinder (10 mm in diameter and 250 mm long). The size of the grains in this sample was of the order of 150 μm and the sample was homogeneous. The concrete sample was in the form of a prism (20 mm × 20 mm basis and 120 mm length). The concrete was more than 5 years old and kept in a lab (room environment). It was composed of sand aggregates only, with grain sizes smaller than 500 μm. No information was available regarding density or porosity.

Both samples were suspended horizontally (see Figure 1a) and put in a climate chamber to allow for humidity control (kept fixed within the experiment at 45 %) and our choice of temperature (varied from 278 K to 303 K, or equivalently from 5 to 30 °C). The suspended configuration enabled almost optimal free-free boundary conditions, which means that a reflection coefficient of the propagating wave at the ends of the sample close to 1 is obtained. Also, effects on the resonance frequency of transducers could be considered minimal.

Samples have been equipped with two piezoelectric transducers (Matest C370-02, Arcore, Italy, with resonance frequency of 55 kHz), glued to the base of the sample by means of phenyl salicylate. Both transducers (acting as generator and receiver, respectively) were connected to a TiePie HS5 oscilloscope-generator (Sneek, The Netherlands) controlled

by Matlab R2022a. The signal generated by the arbitrary waveform generator was amplified by 20 times (power amplifier F20AD) to increase the excitation amplitude voltage. Sampling rate was set to 20 MSa/s. A schematic description of the set-up is shown in Figure 1b.
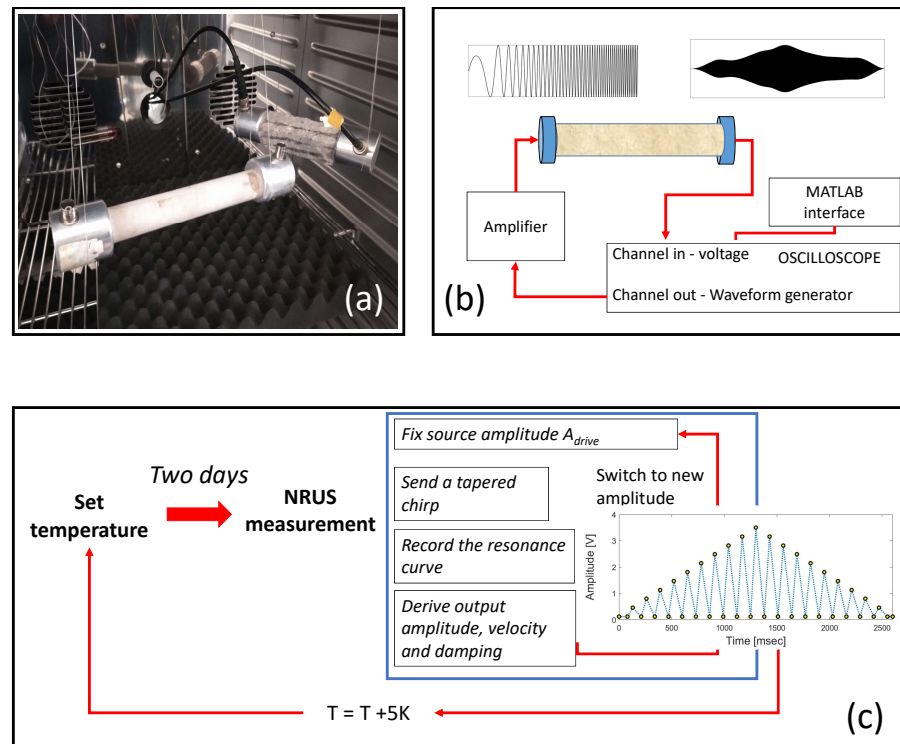
Figure 1. Experimental set-up. (**a**) Image of the suspended samples; (**b**) schematic description of the set-up. Input (schematic) and output (real data) signals are shown in insets; (**c**) representation of the experimental protocol. In the inset, the drive amplitude protocol is shown: conditioning amplitudes (A_{cnd}), increasing up to $A_{\max}$, are alternated with constant baseline amplitudes (A_{baseline}).

2.2. Measurement Protocol

The experiment was conducted as follows (see Figure 1c). Samples were put in the climate chamber and the temperature was set to a given value for about 2 days. Elastic parameters were monitored during thermal relaxation and found to reach an equilibrium value in about 1.5 days, thus ensuring thermal equilibrium before the NRUS measurements were performed roughly 5 days after. Afterwards, temperature was changed to a new value. Initial temperature was 278 K and was increased by 5 K at each step.

Each NRUS acquisition (i.e. for one drive amplitude) consisted of the following steps (and discussed in detail in the following subsection): choice of drive amplitude and injection of a chirp signal; measurement of the received signal; derivation of the resonance curve; and determination of strain amplitude, velocity, and damping. The NRUS measurement consisted of repeating the procedure and varying the drive amplitude. In this work, a baseline loading/unloading amplitude protocol was chosen (also shown in Figure 1c), which consists of alternating high conditioning and low baseline amplitudes, keeping the latter constant (A_{baseline} in the order of tenths of volts) and increasing the first (A_{cnd}) in equal steps up to a maximum value of the order of a few volts (loading phase) and then decrease it back to A_{baseline}. A total of 21 steps for A_{cnd} were chosen.

Each NRUS sequence had the same duration and each probing had a fixed temporal length $\Delta t = 50$ ms, with pauses between successive sweeps at different drive amplitudes to ensure accurate timing control, fundamental for a correct evaluation of slow dynamic effects.

The baseline and maximum conditioning amplitude differed for each temperature/sample and were chosen to guarantee output amplitudes (i.e., strain) in similar ranges.

2.3. Nonlinear Resonant Ultrasonic Spectroscopy Acquisition

Nonlinearity was determined by analyzing the wave propagation velocity dependence on strain. To this purpose, Nonlinear Resonant Ultrasonic Spectroscopy (NRUS) was used. The method consists of measuring the resonance spectra and varying the amplitude of excitation and measuring the resonance frequency and resonance amplitude for each excitation.

To determine the resonance spectra, a tapered chirp excitation was used to sweep over one longitudinal resonance peak:

$$u(t) = A_{\text{drive}} \cos\left(2\pi\left(f_{\min} + \frac{f_{\max} - f_{\min}}{\Delta t}t\right)t\right). \tag{1}$$

The sweep was performed round a resonance mode ($f_{\min} \leq f_{\text{res}} \leq f_{\max}$, where f_{res} is the resonance frequency). The bandwidth of the chirp spectra ($f_{\max} - f_{\min}$) was kept constant at 2.5 kHz, as was the duration $\Delta t = 50$ ms. This choice allowed for accurate resolution of the resonance peak. A discrete Fourier transform with 2 Hz spacing was computed for each response signal, followed by a deconvolution of the chirp spectrum, resulting in the elimination of spectral ripples and normalization of spectral amplitudes. This normalization ensured alignment between the spectral amplitude and the amplitude of the observed signal.

The NRUS sequence consisted of selecting the drive amplitude A_{drive} (following the protocol in Figure 1c, i.e., alternating baseline and conditioning amplitudes). For each amplitude, the experimentally obtained spectrum (see Figure 2a) was fit with the MoDaNE solution [41]:

$$B(f) = \frac{U_0}{\sqrt{\cosh^2[\alpha L] - \cos^2\left[2\pi\left(f + \psi(f - \frac{nv}{2L})^2\right)L/v\right]}}, \tag{2}$$

where f is frequency, n is the mode number, B is the amplitude and L is the sample length. The fit parameters U_0, α, and v correspond to the uncalibrated source amplitude, damping coefficient, and wave velocity, respectively. The term proportional to ψ is a tilting term, which allows one to account for the sensitivity curve of transducers; ψ is thus not a material property. The resonance frequency of the sample is function of one of the fit parameters: $f_{\text{res}} = nv/2L$.

Repeating the procedure for different drive amplitudes, velocities, and damping was performed as a function of output amplitude, which is defined as the maximum of B, i.e., the amplitude at the resonance frequency. Thus, it is derived as follows:

$$A_{\text{out}} = \max(B) = \frac{U_0}{\sqrt{\cosh^2(\alpha L) - 1}}. \tag{3}$$

The output amplitudes, from now on simply called amplitudes, are reported in volts, but, at least in the linear approximation, they are proportional to the strain amplitude in the center of the sample. Since our experiment is not calibrated, it was not possible to convert the voltage to strain, so whenever the term strain is used, it is intended as voltage.

The amplitude A_{out} was derived for all drive amplitudes, both conditioning and baseline. Thus, it provided the definition of the conditioning strain and the baseline strain

in the material. In the following, velocity variations will be plotted as a function of the output conditioning strain.
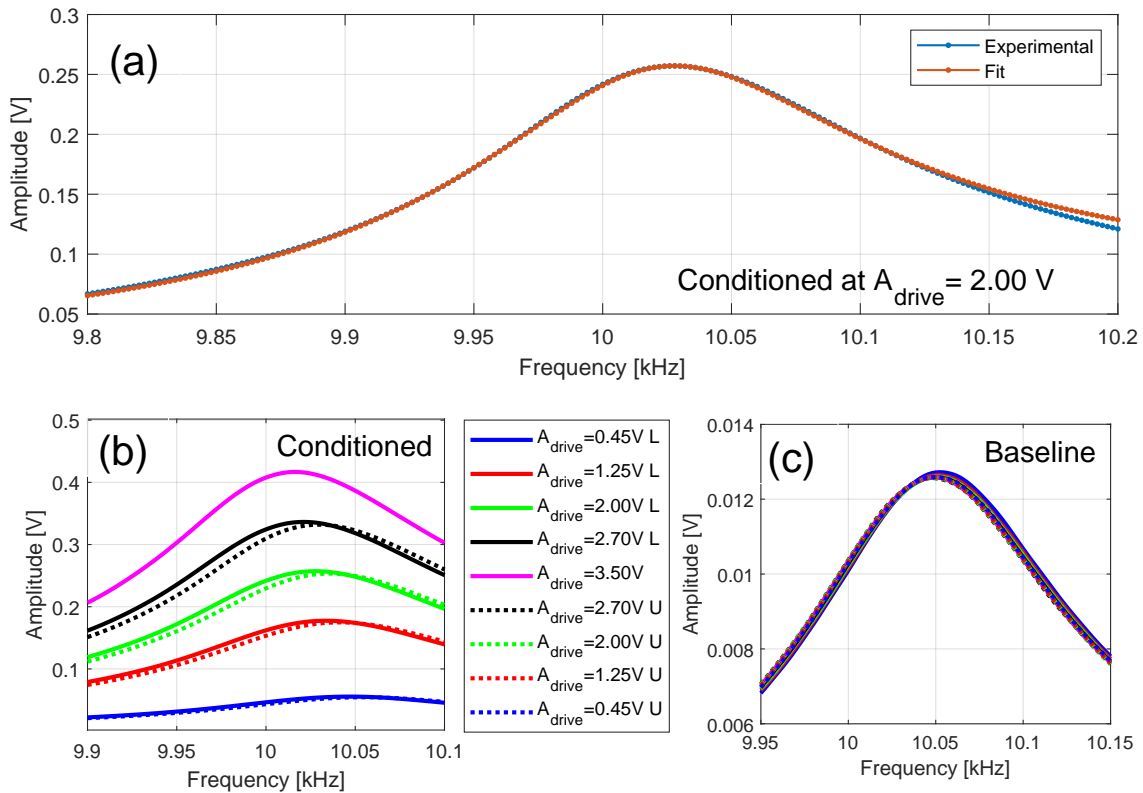
Figure 2. Spectra for concrete at $T = 298$ K. (**a**) Superposition of experimental data and fit (using Equation (2)) for a given drive amplitude. (**b**) Conditioning spectra for selected drive amplitudes. (**c**) Baseline spectra for the same drive amplitudes as in (**b**). Colors indicate the drive amplitudes, solid lines refer to loading, and dashed lines refer to unloading. For the description of subplots (**b**,**c**), refer to Section 3.

2.4. Testing and Repeatability

At each temperature, several repeated NRUS measurements were performed on both samples. A few repeated measurements (between 5 and 10) were performed one after the other and averaged to increase signal-to-noise ratio. The procedure was then repeated (from 5 to 10 times) in successive days and/or changing A_{baseline} and/or A_{max}, to verify repeatability of the experiment. Excellent repeatability was obtained, thus ensuring the robustness of the data analysis performed in the next section (see Appendix A for results).

The second issue faced was testing the eventual deterioration of the transducer bonding. To this purpose, two additional measurements at $T = 293$ K were performed. One before beginning the experimental protocol and one after its end (thus reducing T from 303 back to 293 K). The repeatability of the results ensured that no change in the transducer's quality occurred (one Czech sandstone sample was also tested, but it failed the transducer quality testing and, thus, the corresponding results were discarded). Also, it proved that no damage was generated in the samples.

3. Experimental Results

3.1. Resonance Curves

For each temperature (and each sample), the NRUS protocol allowed the resonance curves (output amplitudes vs. frequency) to be plotted for different conditioning drive amplitudes A_{cnd}. Also, resonance curves at baseline drive amplitude (immediately following

the conditioning phase) were derived. A few selected curves (for concrete at $T = 293$ K) are shown in Figures 2b and 2c, respectively.

As expected, subplot (b) shows a decrease in the resonance frequency and an increase in the peak width and asymmetry with increasing drive amplitude (solid lines). When the measurement protocol consists of an upward-trending and downward-trending sequence of drive amplitudes $A_{\text{drive}} = A_{\text{cnd}}$ in Equation (1), a difference between the results for equivalent amplitudes is present (compare solid with dashed lines), which indicates hysteresis. The behavior of the baseline strain (panel (c)) is also consistent with other measurements: slow dynamics is responsible for the softening and damping increase observed at a constant (low) excitation amplitude ($A_{\text{drive}} = A_{\text{baseline}}$) after conditioning at different drives.

3.2. Velocity and Damping Dependence on Strain

Velocity and damping could be derived (using MoDaNE fitting, as discussed in Section 2.3) and plot vs. output amplitude (strain). In the following, data referring to velocity are discussed, but the same applies to damping as well. It is possible to introduce the conditioned and baseline relative velocity variations:

$$\delta v_{\text{C,B}} = \frac{v_{\text{C,B}} - v_{\text{lin}}}{v_{\text{lin}}}, \tag{4}$$

where v_{lin} is the linear velocity at the given temperature, measured by exciting the sample at a very low excitation amplitude (smaller than or equal to the baseline drive amplitude). Note that Equation (4) applies to both the conditioned and baseline states, thus justifying the notation used for the pedices.

The velocity measured at conditioning strain δv_{C} contains contributions from both fast and slow dynamics. Separating the two terms is desirable, since they might (or might not) originate from different physical mechanisms and, depending on the driving parameter (which, here, is temperature) the relative weight of the two contributions might change. Furthermore, slow dynamics-related effects strongly depend on the experimental set-up properties and, thus, it is advisable to remove them to obtain observations that are only "sample-dependent".

During conditioning at a given drive amplitude, a contribution to the velocity variation, larger for larger amplitudes, is slowly built up over time. As soon as the excitation is switched to the baseline amplitude, this contribution slowly relaxes back to zero. Therefore, slow dynamics originates a contribution which increases with the duration of the drive [1] and is due to the evolution of the material properties towards a strain-dependent equilibrium state, which is only partially achieved in the Δt defining the duration of the chirp. The slow contribution does not disappear instantly; thus, it contributes to the determination of the velocity measured at baseline (low amplitude) drive. Assuming the relaxation of the slow dynamic contribution before probing the baseline to be small, the fast contribution to velocity variation can be defined as

$$\delta v_{\text{fast}} = \delta v_{\text{C}} - \delta v_{\text{B}} = \frac{v_{\text{C}} - v_{\text{B}}}{v_{\text{lin}}}. \tag{5}$$

In Figure 3, the strain dependence of conditioned, baseline, and fast velocity variations are reported compared to the strain (output amplitude). The results show some common features in the behavior of the velocity variation vs. strain for Berea and concrete:

- δv_{C}: hysteresis is present, given by the difference between the loading and unloading branches;
- δv_{B}: besides the hysteresis (which is even more remarkable than in the conditioned data), it can be observed that the maximum baseline velocity variation does not

occur when the conditioning strain is maximum; see the further decrease in velocity observed during the first instances of unloading (blue symbols);

- δv_{fast}: the hysteresis, and hence, slow dynamic effects, is completely removed.
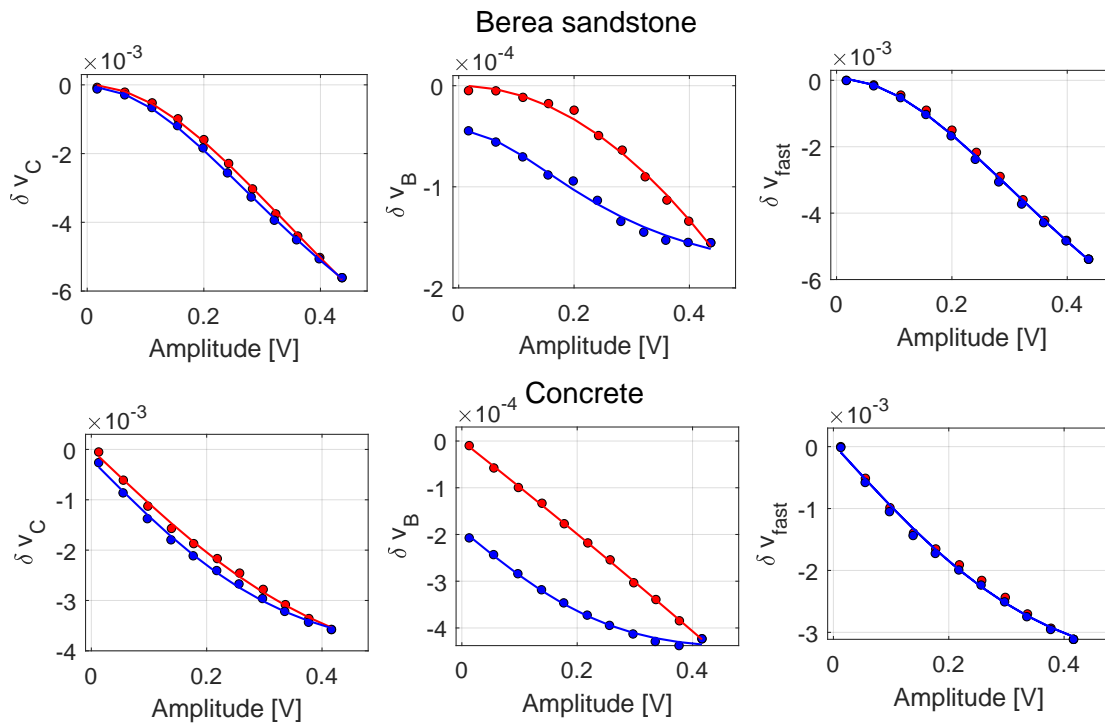
Figure 3. Velocity variations vs. conditioning strain. δv_{C} and δv_{B} are the conditioned and baseline velocity variations, respectively. δv_{fast} is the fast dynamic contribution to the velocity variation (see Equation (5)). Red symbols refer to loading (drive amplitude increases), while blue ones to unloading (drive amplitude decreases). Data reported refer to measurements performed at $T = 283$ K. Here, the x-axes (strain) correspond to the output amplitude (in volts) defined by Equation (3), when $A_{\text{drive}} = A_{\text{cnd}}$.

However, apparent changes in the functional form of the dependence can be observed. At first glance, a quadratic dependence seems to be shared by all curves, but with positive/negative quadratic terms for concrete/Berea. All data (except unloading data for concrete) also seem to present a strain interval in which the behavior is linear. This wealth of behaviors is indeed reflective of the complexity of NRUS data, which can be found in the literature. At least for Berea, depending on the strain testing range, different authors have observed quadratic, linear or S-shaped behaviors [1,42–45]. It is our assumption here that the latter might be a better representation of the velocity dependence on strain. This is definitely true for Berea, but most likely also for concrete, except that the baseline amplitude used for concrete was perhaps too high, thus not allowing for the detection of bending with early strain. More details about the fitting procedure are given in Appendix B.

Based on this assumption, curves have been fit with a sigmoidal-like function defined as

$$\delta v(A) = \frac{a_1 A + a_2 A^2}{1 + a_3 A^2}, \tag{6}$$

where a_1 and a_2 are negative parameters, while a_3 is a positive parameter. The fitting obtained using Equation (6) is shown as solid lines in Figure 3 and it is remarkable how the same function allows for the optimal fitting of both the loading and unloading branches of the curves. Note that, for the fast velocity variations, all the data have been fit with a single "sigmoidal", with the two branches being superimposed.

As mentioned, similar conclusions can be derived for damping, as shown in Appendix C.

4. Temperature Dependence

4.1. Temperature Dependence of Linear Elastic Parameters

The procedure proposed allows us to determine, for each temperature, the linear viscoelastic (velocity and damping) parameters. Indeed, by extrapolating the curves of the velocity and damping versus strain to zero strain, it is feasible to obtain a prediction of the material parameters in the unperturbed state. The results are reported in Figure 4.
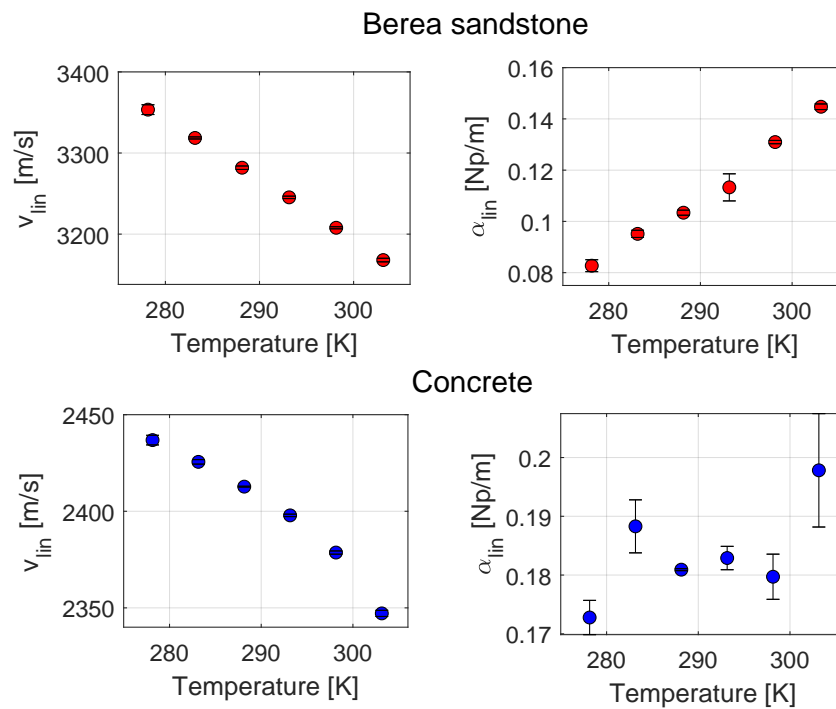
Figure 4. Linear viscoelastic parameters vs. temperature: velocity (**left**) and damping (**right**). Data are averaged over repetitions of the experiment and the errorbar is given by the semidispersion.

As expected, the material becomes softer (the velocity diminishes) for both the Berea and concrete. A significant reduction (a few percent) is observed. In particular, the velocity decrease is 5.5 percent for Berea and 3.6 percent for concrete. The behavior of damping is different for the two materials. In the case of Berea, the damping coefficient α_{lin} increases significantly (81 percent), while for concrete, no significant trend as a function of temperature is appreciable.

4.2. Temperature Dependence of Nonlinear Fast Elastic Parameters

Curves reporting the velocity variation dependence on strain are obtained for each temperature. The focus in this work is only on the fast contributions to nonlinearity (δv_{fast}) and results for Berea and concrete are reported in Figure 5. In the case of Berea, a notable effect is observed, with relative velocity variations that nearly double within the temperature range considered. On the contrary, no trend is observed for concrete; thus, fast nonlinearity seems to be temperature-independent.

Curves reported in Figure 5 are all well fit by the sigmoidal-like function proposed herein (Equation (6)). The fit is shown by a continuous line in the plots. Thus, the fitting parameters a_1, a_2 and a_3 could be used to quantify the nonlinearity dependence on temperature. Rather than discussing the dependence of the parameters on temperature, the authors

prefer to consider some of the properties of the fitting curves in Equation (6), which are more meaningful:

- The asymptotic value given by a_2/a_3, which represents the upper limit of velocity variations for large strains (note that the sigmoidal-like behavior is expected to be valid only till a maximum strain range, beyond which other mechanisms might take place and, thus, such asymptotic value does not really exist);
- The inflection point of the curves, obtained by setting to zero the second derivative of Equation (6);
- The slope of the linear approximation around the inflection point, given by the value of the derivative of Equation (6) at the inflection point. This value could be considered as the equivalent of the hysteretic parameter α often used in NRUS measurements, even though it is uncalibrated here. Recall that the hysteretic parameter α is not related to the damping coefficient used here (and is called α as well).
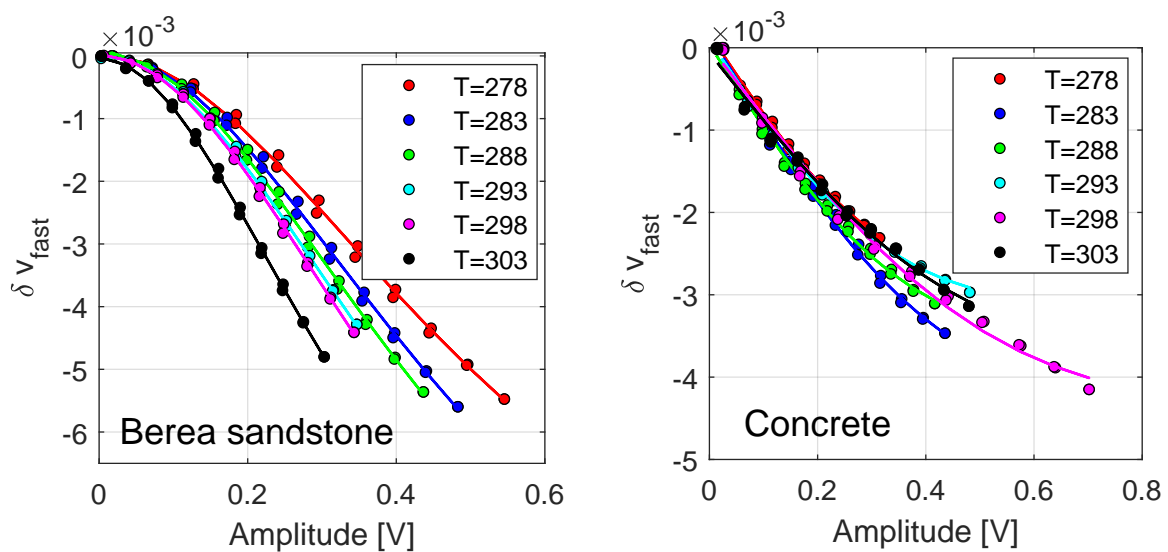
Figure 5. Nonlinear fast velocity variations vs. strain at different temperatures. Here, the x-axes (strain) correspond to the output amplitude (in volts) defined by Equation (3), when $A_{\text{drive}} = A_{\text{cnd}}$.

The nonlinear properties vs. temperature for Berea are reported in Figure 6. As expected, the nonlinearity increases with temperature, while the inflection point moves to lower strain amplitudes. The slope (somehow similar to the hysteretic parameter α) increases (in modulus) with temperature, with an increase of about 50 percent. Of course, no temperature dependence trend is observed for concrete.

The results for damping are discussed in Appendix C.

### 4.3. Temperature Dependence of Slow Dynamic Parameters

When considering the strain dependence of the conditioned velocity (see Figure 3), two properties of the curves are related to slow dynamic effects: the area of the loop and the residual velocity variation when the amplitude returns to zero in the unloading phase (intersection with the y-axes). The two parameters are shown against temperature in Figure 7. Stronger effects due to slow dynamics in the concrete sample compared to Berea can be appreciated (see the scales on the axes).

The situation for what dictates the slow dynamic parameters' dependence on temperature is different. A clear trend with temperature is observed for Berea, exhibiting a reduction in slow dynamic effects, which, despite the large error bars, seems to be reliable. For concrete, no clear trend could be identified, since, especially for residuals data, slow dynamics seem to be unaffected by temperature variations.
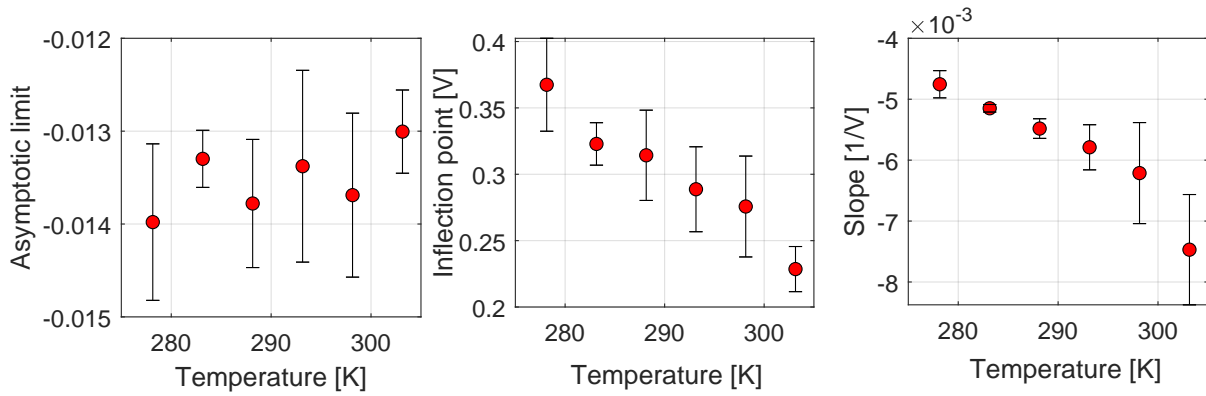
Figure 6. Nonlinear fast elastic parameters vs. temperature. Data are averaged over repetitions of the experiment and the errorbar is given by the semidispersion. Data refer to the Berea sandstone sample.

The strongest conditioning observed in the concrete, corresponding to the fact that it is temperature-independent, may be due to several causes. In our opinion, it is possible that the observation is due to the different roles of water in the two materials. A higher water mobility might indeed result in a stronger dependence of the strength of slow dynamics' contribution to external parameters like the temperature. While, in a more chemically active system, like concrete, the presence of water might produce stronger non-equilibrium effects.
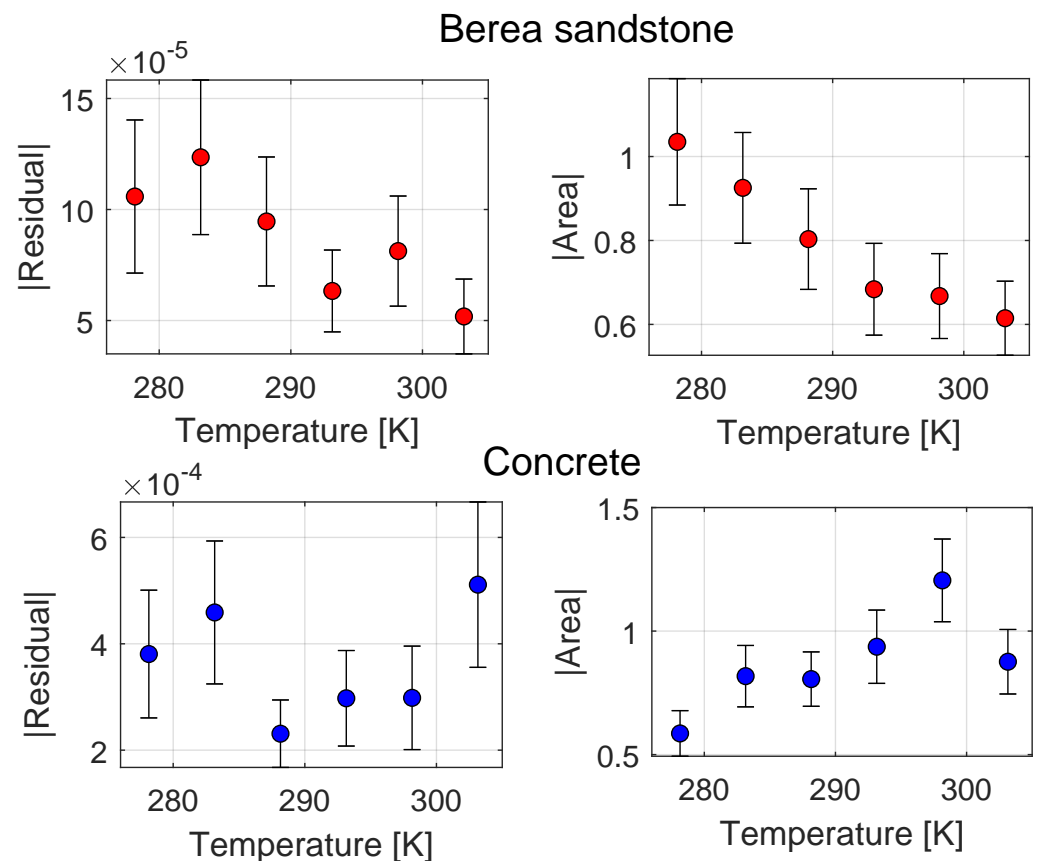
Figure 7. Slow dynamic parameters vs. temperature. Data are averaged over repetitions of the experiment and the errorbar is given by the semidispersion. Note that the area of the loops has the dimension of volts.

5. Conclusions and Discussion

In this paper, the temperature dependence in the ambient range of both the linear and nonlinear elastic parameters of Berea sandstone and concrete was studied. A novel procedure was introduced to extract velocity and damping variations as a function of the strain amplitude, which allows one to distinguish fast nonlinearity effects (Figure 6) from slow ones (Figure 7). Parameters have been defined to quantify the observed effects: the inflection point and slope of the velocity's dependence on amplitude (fast) and the residual effects of conditioning and the area of the hysteretic loop (slow). The authors did not find a universal behavior for these two consolidated granular media, except for the decrease with temperature of the linear propagation velocity (Figure 4).

In Berea, linear damping and fast dynamics increase with temperature, while effects due to slow dynamics diminish. This might be due to the fact that, with increasing temperature, the processes responsible for memory, conditioning, and relaxation might occur on a faster time scale. Thus, in a multirelaxation model, more physical features will react faster (compared to period and/or chirp duration) and thus contribute to the fast effect and less so to the slow reaction, thus diminishing long-term effects like memory.

The fact that nonlinear features are temperature-independent in concrete is in parallel with the fact that linear damping is also temperature-independent. The parallelism in the behavior of damping and nonlinear velocity variations could be an indication of some deeper physical aspects responsible of our observations, which, however, needs more data to be investigated. As a hint for future work, it can be speculated that the different behaviors of concrete and Berea, which share a similar microstructure, could be due to the different roles of water (humidity-related) in the two materials.

Appendix A. Repeatability

As mentioned in the text, experiments have been repeated for each temperature, either in successive days or slightly changing the range of drive amplitudes. Results of repeated experiments on Berea are shown in Figure A1. Results for concrete are similar. Excellent repeatability is obtained, the scattering among data at the same temperature (different colors) being negligible when compared to the difference in behavior due to a temperature change.
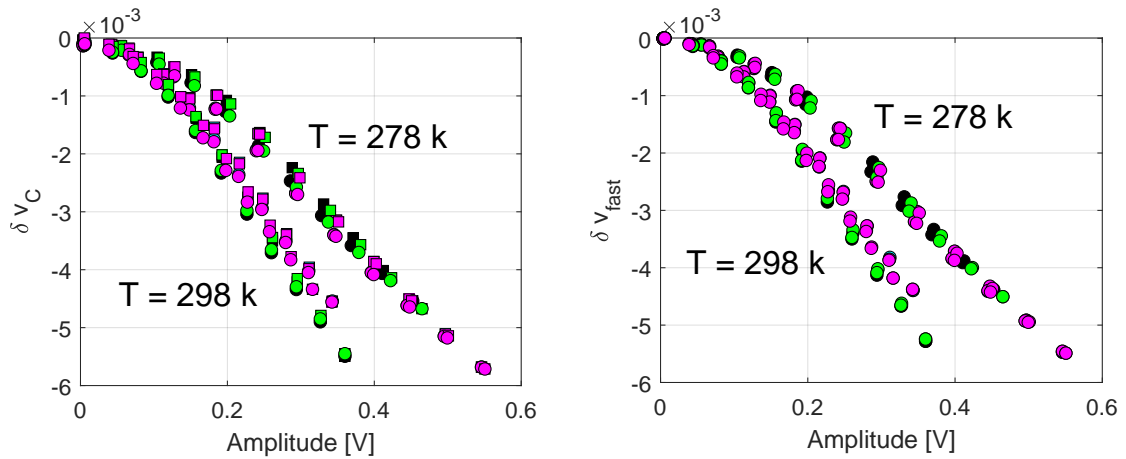
Figure A1. Repeatability of the experiments. Results are reported for Berea sandstone at two different temperatures. Different colors refer to different repetitions. Regarding δv_C, circles and squares refer to loading/unloading branches of the curve.

Appendix B. Fitting

The dependence of velocity variation vs. amplitude is shown for Berea and concrete in Figure A2. As mentioned in the main text, the behavior for the two materials appears different. A quadratic dependence seems to be shared by all curves, but with a positive/negative quadratic term for concrete/Berea, which is hard to explain. As a possible alternative, a sigmoidal-like fit (see Equation (6)) fits all the curves well, with signs of the parameters consistent for the two materials.
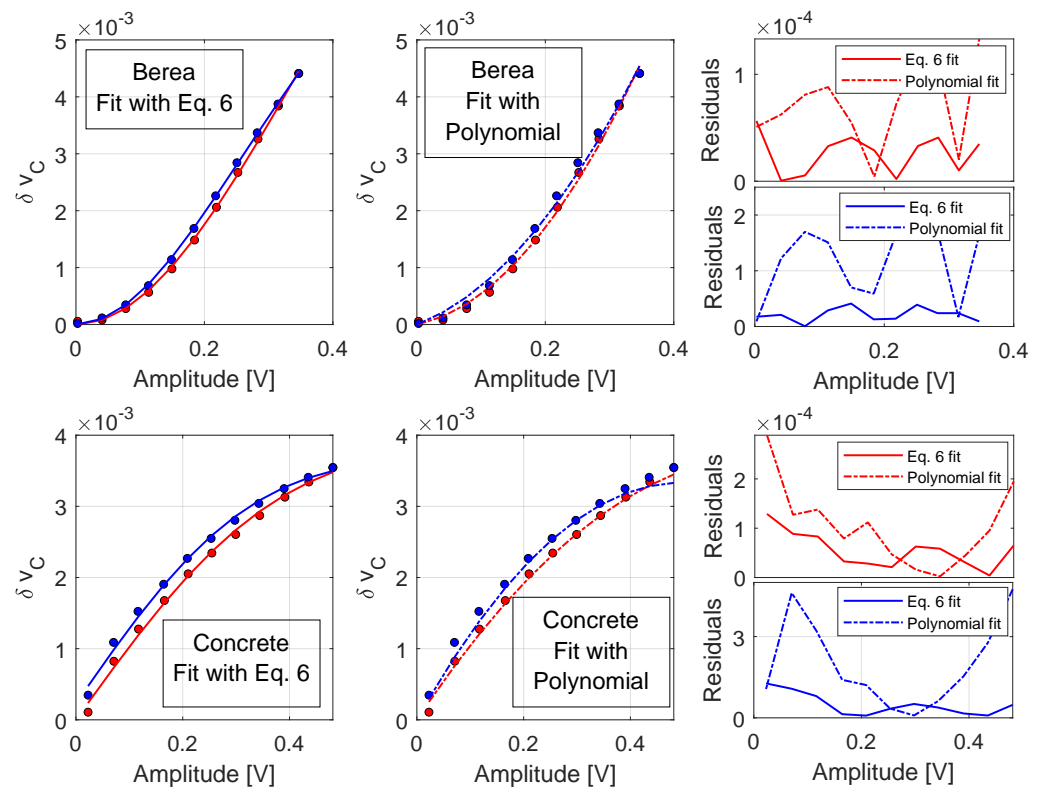

Figure A2. Fitting the velocity variation vs. strain curves for Berea (upper row) and concrete (lower row). Both loading (red) and unloading (blue) experimental data are fit independently using Equation (6) (solid line—left column) or using a quadratic polynomial (dot-dashed line—central column). The residuals are reported for loading and unloading branches in the right column.

Here, the two fitting procedures are compared. Fitting data with a sigmoidal-like function (left column in Figure A2) seems slightly more accurate than fitting with a second-order polynomial fit (central column), particularly for the unloading branch of the curves (blue). The advantages of the sigmoidal-like fitting are even more pronounced when considering the baseline velocity variation (not reported here but shown in Figure 3).

The better quality of the fit using Equation (6) could be better appreciated when calculating the residuals (absolute values of the difference between experimental and fit data). They are shown for Berea and concrete in the right column of Figure A2. Thus, the advantages of the proposed sigmoidal-like function, used to fit the data, are two-fold: the fit is slightly more accurate and the function is more universal, in the sense that it fits (with parameters with the same sign) all data well (loading/unloading, conditioned/baseline, velocity/damping).

Appendix C. Damping

In the main text, the dependence of velocity on strain and the dependence on temperature of nonlinear parameters have been analyzed (see Figures 3 and 5, respectively). This approach also allows us to estimate damping. The data for concrete are unreliable due to a high degree of noise (and will not be discussed here). For Berea sandstone, for damping, a similar behavior is observed as for velocity, as shown in Figure A3.
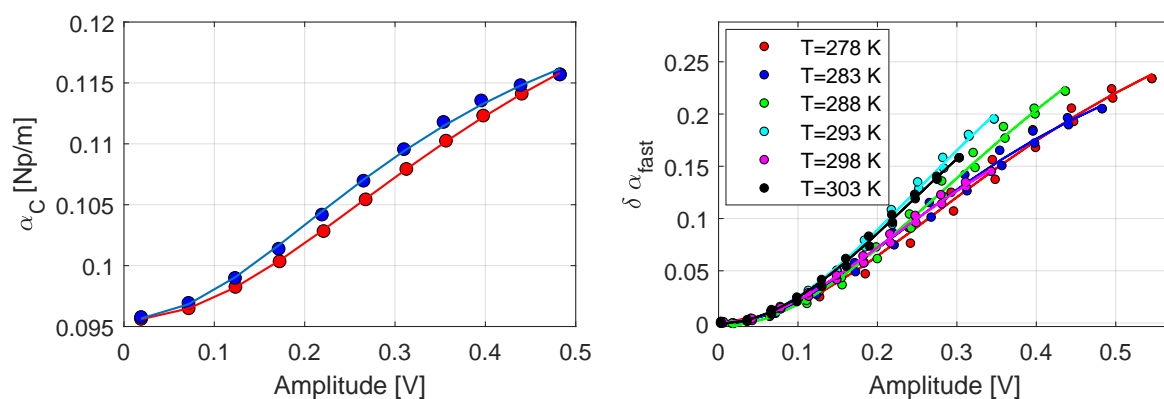
Figure A3. Damping behavior for Berea data. Damping dependence on strain at a fixed temperature (**left**). Note the difference in the loading/unloading branches. Dependence of fast contribution to damping for increasing temperatures (**right**). In both subplots, symbols are experimental data and solid lines are fits using Equation (6).

In particular, as shown in the left subplot, damping depends on strain following a sigmoidal-like curve, as does velocity, which fits well using Equation (6).Furthermore, for both materials, fast contributions to nonlinearity seem independent on temperature (right subplot). Recall that nonlinear velocity variations were found to increase with increasing temperature.

References

1. TenCate, J.A.; Pasqualini, D.; Habib, S.; Heitmann, K.; Higdon, D.; Johnson, P.A. Nonlinear and nonequilibrium dynamics in geomaterials. *Phys. Rev. Lett.* **2004**, *93*, 065501 [CrossRef]
2. Lott, M.; Remillieux, M.C.; Garnier, V.; Bas, P.-Y.L.; Ulrich, T.J.; Payan, C. Nonlinear elasticity in rocks: A comprehensive three-dimensional description. *Phys Rev. Mat.* **2019**, *1*, 023603. [CrossRef]
3. Bittner, J.A.; Popovics, J.S. Direct Imaging of Moisture Effects during Slow Dynamic Nonlinearity. *Appl. Phys. Lett.* **2019**, *114*, 021901. [CrossRef]
4. Riviere, J.; Shokouhi, P.; Guyer, R.A.; Johnson, P.A. A set of measures for the systematic classification of the nonlinear elastic behavior of disparate rocks. *J. Geophys. Res. Solid Earth* **2015**, *120*, 1587. [CrossRef]

5. Scalerandi, M.; Bentahar, M.; Mechri, C. Conditioning and Elastic Nonlinearity in Concrete: Separation of Damping and Phase Contributions. *Constr. Build. Mater.* **2018**, *161*, 208. [CrossRef]

6. Chen, J.; Kim, J.-Y.; Kurtis, K.E.; Jacobs, L.J. Theoretical and experimental study of the nonlinear resonance vibration of cementitious materials with an application to damage characterization. *J. Acoust. Soc. Am.* **2011**, *130*, 2728. [CrossRef]

7. Gliozzi, A.S.; Scalerandi, M.; Anglani, G.; Antonaci, P.; Salini, L. Correlation of elastic and mechanical properties of consolidated granular media during microstructure evolution induced by damage and repair. *Phys. Rev. Mater.* **2018**, *2*, 013601. [CrossRef]

8. TenCate, J.A.; Smith, E.; Guyer, R.A. Universal Slow Dynamics in Granular Solids. *Phys. Rev. Lett.* **2000**, *85*, 1020. [CrossRef]

9. Johnson, P.A.; Sutin, A. Slow dynamics and anomalous nonlinear fast dynamics in diverse solids. *J. Acoust. Soc. Am.* **2005**, *117*, 124. [CrossRef]

10. Muir, T.G.; Cormack, J.M.; Slack, C.M.; Hamilton, M.F. Elastic softening of sandstone due to a wideband acoustic pulse. *J. Acoust. Soc. Am.* **2020**, *147*, 1006–1014. [CrossRef]

11. Scalerandi, M.; Mechri, C.; Bentahar, M.; Bella, A.D.; Gliozzi, A.S.; Tortello, M. Experimental evidence of correlations between conditioning and relaxation in hysteretic elastic media. *Phys. Rev. Appl.* **2019**, *12*, 044002. [CrossRef]

12. Zeman, R.; Kober, J.; Nistri, F.; Scalerandi, M. Relaxation of Viscoelastic Properties of Sandstones: Hysteresis and Anisotropy. *Rock Mech. Rock Eng.* **2024**, *57*, 6701. [CrossRef]

13. Tencate, J.A.; Shankland, T.J. Slow dynamics in the nonlinear elastic response of Berea sandstone. *Geoph. Res. Lett.* **1996**, *23*, 3019–3022. [CrossRef]

14. Trarieux, C.; Callé, S.; Moreschi, H.; Renaud, G.; Defontaine, M. Modeling nonlinear viscoelasticity in dynamic acoustoelasticity. *Appl. Phys. Lett.* **2014**, *105*, 264103. [CrossRef]

15. Snieder, R.; Sens-Schönfelder, C.; Wu, R. The Time Dependence of Rock Healing as a Universal Relaxation Process, a Tutorial. *Geophys. J. Int.* **2017**, *208*, 1. [CrossRef]

16. Shokouhi, P.; Riviere, J.; Guyer, R.A.; Johnson, P.A. Slow Dynamics of Consolidated Granular Systems: Multi-Scale Relaxation. *Appl. Phys. Lett.* **2017**, *111*, 251604. [CrossRef]

17. Kober, J.; Gliozzi, A.S.; Scalerandi, M.; Tortello, M. Material Grain Size Determines Relaxation-Time Distributions in Slow-Dynamics Experiments. *Phys. Rev. Appl.* **2022**, *17*, 014002. [CrossRef]

18. Chavazas, M.L.; Bromblet, P.; Berthonneau, J.; Hénin, J.; Payan, C. Impact of relative humidity variations on Carrara marble mechanical properties investigated by nonlinear resonant ultrasound spectroscopy. *Constr. Build. Mat.* **2024**, *431*, 136529. [CrossRef]

19. Maier, S.; Kim, J.Y.; Forstenhäusler, M.; Wall, J.J.; Jacobs, L.J. Noncontact nonlinear resonance ultrasound spectroscopy (NRUS) for small metallic specimens. *NDT E Int.* **2018**, *98*, 37–44. [CrossRef]

20. Bentahar, M.; El Aqra, H.; El Guerjouma, R.; Griffa, M.; Scalerandi, M. Hysteretic elasticity in damaged concrete: Quantitative analysis of slow and fast dynamics. *Phys. Rev. B* **2006**, *73*, 014116. [CrossRef]

21. Bruno, C.L.E.; Gliozzi, A.S.; Scalerandi, M.; Antonaci, P. Analysis of elastic nonlinearity using the Scaling Subtraction Method. *Phys. Rev. B* **2009**, *79*, 064108. [CrossRef]

22. Ohara, Y.; Shintaku, Y.; Horinouchi, S.; Ikeuchi, M.; Yamanaka, K. Enhancement of Selectivity in Nonlinear Ultrasonic Imaging of Closed Cracks Using Amplitude Difference Phased Array. *Jap. J. Appl. Phys.* **2012**, *51*, 07GB18. [CrossRef]

23. Van den Abeele, K.; Carmeliet, J.; Cate, J.A.T.; Johnson, P.A. Nonlinear Elastic Wave Spectroscopy (NEWS) Techniques to Discern Material Damage, Part II: Single-Mode Nonlinear Resonance Acoustic Spectroscopy. *Res. Nondestruct. Eval.* **2000**, *12*, 31. [CrossRef]

24. Chen, J.; Yin, T.; Kim, J.-Y.; Zheng, X.; Yao, Y. Characterization of thermal damage in sandstone using the second harmonic generation of standing waves. *Int. J. Rock Mech. Min. Sci.* **2017**, *91*, 81–89. [CrossRef]

25. van den Abeele, K.; De Visscher, J. Damage assessment in reinforced concrete using spectral and temporal nonlinear vibration techniques. *Cem. Concr. Res.* **2000**, *30*, 1453–1464. [CrossRef]

26. Antonaci, P.; Bruno, C.L.E.; Gliozzi, A.S.; Scalerandi, M. Evolution of damage-induced nonlinearity in proximity of discontinuities in concrete. *Int. J. Solids Struct.* **2010**, *47*, 1603–1610. [CrossRef]

27. Scalerandi, M.; Griffa, M.; Antonaci, P.; Wyrzykowski, M.; Lura, P. Nonlinear elastic response of thermally damaged consolidated granular media. *J. Appl. Phys.* **2013**, *113*, 154902. [CrossRef]

28. Payan, C.; Garnier, V.; Moysan, J. Applying nonlinear resonant ultrasound spectroscopy to improving thermal damage assessment in concrete. *J. Acoust. Soc. Am.* **2007**, *121*, EL125. [CrossRef]

29. Simpson, J.; van Wijk, K.; Adam, L.; Esteban, L. Temperature-Induced Nonlinear Elastic Behavior in Berea Sandstone Explained by a Modified Sheared Contacts Model. *J. Geophys. Res.-Solid Earth* **2023**, *128*, B025452. [CrossRef]

30. Boukari, Y.; Bulteel, D.; Rivard, P.; Abriak, N.-E. Combining nonlinear acoustics and physico-chemical analysis of aggregates to improve alkali-silica reaction monitoring. *Cem. Concr. Res.* **2015**, *67*, 44–51. [CrossRef]

31. Antonaci, P.; Bruno, C.L.E.; Scalerandi, M.; Tondolo, F. Effects of corrosion on linear and nonlinear elastic properties of reinforced concrete. *Cem. Concr. Res.* **2013**, *51*, 96–103. [CrossRef]

32. Bouchaala, F.; Payan, C.; Garnier, V.; Balayssac, J.P. Carbonation assessment in concrete by nonlinear ultrasound. *Cem. Concr. Res.* **2011**, *41*, 557–559. [CrossRef]

33. Johnson, P.A.; Zinszner, B.; Rasolofosaon, P.; Cohen-Tenoudji, F.; Van Den Abeele, K. Dynamic measurements of the nonlinear elastic parameter α in rock under varying conditions. *J. Geophys. Res.-Solid Earth* **2004**, *109*, B02202. [CrossRef]

34. Gao, L.Y.; Shokouhi, P.; Riviere, J. Effect of relative humidity on the nonlinear elastic response of granular media. *J. Appl. Phys.* **2022**, *131*, 055101. [CrossRef]

35. Manogharan, P.; Wood, C.; Marone, C.; Elsworth, D.; Rivière, J.; Shokouhi, P. Experimental Investigation of Elastodynamic Nonlinear Response of Dry Intact Fractured and Saturated Rock. *Rock Mech. Rock Eng.* **2021**, *5*, 2665–2678. [CrossRef]

36. Ulrich, T.J.; Darling, T.W. Observation of anomalous elastic behavior in rock at low temperatures. *Geophys. Res. Lett.* **2001**, *28*, 2293. [CrossRef]

37. Nobili, M.; Scalerandi, M. Temperature effects on the elastic properties of hysteretic elastic media: Modeling and simulations. *Phys. Rev. B* **2004**, *69*, 104105. [CrossRef]

38. Feng, X.; Fehler, M.; Burns, D.; Szabo, S.B.T.L. Effects of humidity and temperature on the non-linear elasticity of rocks. *Geophys. J. Int.* **2022**, *231*, 1823–1832. [CrossRef]

39. Zou, G.; Zeng, H.; Gong, F.; Yin, C.; Li, S.; Peng, S.; Xu, Z. Effects of temperature and water saturation on the elastic moduli of sandstone and mudstone from the Lufeng geothermal field: Experimental results and theoretical model. *Geophys. J. Int.* **2022**, *230*, 1147–1165. [CrossRef]

40. Davis, E.S.; Sturtevant, B.T.; Sinha, D.N.; Pantea, C. Resonant Ultrasound Spectroscopy studies of Berea sandstone at high temperature. *J. Geophys. Res.-Solid Earth* **2016**, *121*, 6401–6410. [CrossRef]

41. Di Bella, A.; Gliozzi, A.S.; Scalerandi, M.; Tortello, M. Analysis of Elastic Nonlinearity Using Continuous Waves: Validation and Applications. *Appl. Sci.* **2019**, *9*, 5332. [CrossRef]

42. Rivière, J.; Renaud, G.; Guyer, R.A.; Johnson, P.A. Pump and probe waves in dynamic acousto-elasticity: Comprehensive description and comparison with nonlinear elastic theories. *J. Appl. Phys.* **2013**, *114*, 054905. [CrossRef]

43. Gregg, J.F.; Anderson, B.E.; Remillieux, M.C. Electromagnetic excitation technique for nonlinear resonant ultrasound spectroscopy. *NDT E Int.* **2020**, *109*, 102181. [CrossRef]

44. Remillieux, M.C.; Guyer, R.A.; Payan, C.; Ulrich, T.J. Decoupling Nonclassical Nonlinear Behavior of Elastic Wave Types. *Phys. Rev. Lett.* **2016**, *116*, 115501. [CrossRef] [PubMed]

45. Mashinskii, E.I. Nonlinear amplitude–frequency characteristics of attenuation in rock under pressure. *J. Geophys. Eng.* **2006**, *3*, 291–306. [CrossRef]